

IMPLEMENTATION OF A LOW COST STRUCTURED LIGHT SCANNER

M. Pashaei *, S.M. Mousavi

Faculty of Engineering, University of Tehran, Tehran, Iran - (mpashae, smmousavi)@ut.ac.ir

KEY WORDS: Cultural Heritage, 3D Reconstruction; Stereo Vision; Coded structured light; Stereo Matching; System Calibration; Essential matrix; Line shift processing

ABSTRACT:

In this paper, a practical 3D scanner based on coded structured light principle is reported. The system integrates the technology of close range photogrammetry and Gray code structured light together with multi-line shift processing methodology. This 3D acquisition device allows building highly dense and accurate models of real world in a cost- and time-effective manner. The configuration consists of a digital multimedia projector and two digital cameras. One advantage of this configuration is, that the projection device can, but is not required to be stable over time nor it does have to be calibrated. Given a point on left image, the correspondent point on right image is the intersection of coded light stripes with the same code and epipolar line. Then, the depth is estimated by triangulation. The experimental results have shown that, the proposed solution for essential matrix derivation and applying it to find correspondent points throughout Grey coded multi-line data sets yields high accuracy and density surface reconstruction with the lowest percentage of mismatch or blunder even for semi-complex objects. Some other advantages of this system lie in its design simplicity, low cost and the potential for fast and robust implementation.

1. INTRODUCTION

One of the most important goals in Cultural Heritage applications is 3D digitization of artefacts such as sculptures and epigraphs carved into stones and some walls of historical buildings.

Traditional 3D modeling tools and approaches result inadequate to model the shape of the art works of interest in Cultural Heritage applications. Due to the shape complexity and/or poor texture in some area of most artefacts and also to the accuracy requested. The 3D model in many cases should not only look visually similar to the real object, but should also be very accurate, from a geometrical point of view.

Stereo vision, a most fundamental method in the field of close range photogrammetry, plays an important role in 3D object model recovery from a series of images obtained from different viewpoints. 3D information is obtained by identifying common features in two images. Compared with the active methods, stereo vision is a low cost method in terms of system setup. Unfortunately, finding the correspondences (stereo matching) for each image point is known to be difficult due to image noise, untextured regions and occlusions. Some techniques, such as correlation based techniques (Fusiello, 1997), and multi-resolution techniques (Sun, 1997), have been developed to provide robust or fast stereo matching.

Coded structured light is an active stereovision technique which aims to maximise the number of correspondences that can be obtained in every image. A basic structured light sensor usually consists of one camera and one projector which together form an active stereo pair. Unlike passive stereo which uses two cameras, a structured light sensor generates dense world points

by sampling image points on the light stripe in the image, and totally avoids the so-called correspondence problem. In addition, a structured light sensor can achieve some important features like: large number of 3D reconstructed points well distributed over the measuring surface and good accuracy in the 3D measurements.

To design and use a structured light sensor, three main aspects need to be made efforts on: sensor structure design, sub-pixel center localization of the light stripe and calibration. To be more specific, first, three sensor structure parameters mostly affect the sensor measurement accuracy, i.e. the angle between the optical axis of the camera and the light plane, the distance (called base line) between the camera optical center and the structured light source, and the ratio of the depth of the measured point to the effective focal length of the camera. Second, sub-pixel image coordinates of the light stripe need to be localized in order to guarantee both the sensor calibration accuracy and measurement accuracy. Third, methods of calibration are critical for successful measurement and easy operation on spot.

Here, we design a low-cost vision sensor that can efficiently acquire dense 3D data of complex objects. The sensor combines the technologies of photogrammetric stereo vision and Gray code structured light together with multi-line shift processing, of which the latter simplifies the process of finding correspondence.

Left camera and right camera in stereo vision simultaneously capture coded light and multi-line structured light patterns on a measured object. According to these coded light patterns, every light stripe in images captured by the two cameras is encoded with a unique code. Given a light stripe point on left image, the

correspondent point on right image is the intersection of light stripe with the same code and epipolar line.

Currently, there are many methods for encoding structured lights. Salvi et al, 2004, classify the coding methods into three types: (1) time-multiplexing; (2) neighborhood codification; and (3) direct codification. Time-multiplexing is one of the most commonly used coding strategies based on temporal coding. In this case, a set of patterns is successively projected onto the measuring surface. The codeword for a given pixel is usually formed by the sequence of illumination values for that pixel across the projected patterns. Neighborhood codification tends to concentrate all coding scheme in a unique pattern. The codeword that labels a certain point of the pattern is obtained from a neighborhood of the points around it. As for direct codification, there are certain ways of creating a pattern so that every pixel can be labeled by the information represented on it. In order to achieve this, it is necessary to use either a large number of color values or introduce periodicity. In order to solve the correspondence problem fast and precisely and also to acquire more dense 3D data, we applied an efficient method based on the combination of Gray code and line-shift processing (Guhring, 2001). Each of the lines can be effortlessly encoded by the Gray code method.

This paper is organized as follows: Section 2 introduces the principle of the coded structured light based photogrammetric stereo vision system. In Section 3, we describe the system calibration process and the basic concepts that will be used in formulating our methodology to compute the essential matrix. Section 4 outlines the method of extracting light stripe. In Section 5, we detail our methods about finding correspondences, including two parts: encoding stripes and solving intersection. The experiment and results are given in Section 6. Finally, the conclusion is given in Section 7.

2. SYSTEM OVERVIEW

The structure of measurement system is shown in Figure. 1. The scanner has been designed around two very common electronic devices: a DLP multimedia projector and two digital cameras which compose a stereo vision system. After camera calibration process to determine intrinsic parameters of each camera, the two cameras are mounted on a stable aluminum profile with a fixed, but unknown, relative orientation. The video projector is used to project structured light patterns on the object to be scanned, simultaneously captured by the two cameras. It has to be noted that in contrast to using a specialized stripe projector, which is more stable over time, only the cameras are calibrated. In this setup, the projector is only used as an aid to establish point correspondences. The two digital cameras and the video projector constitute a vision sensor. Both devices are driven by a software tool running on a standard PC, which produces the series of patterns projected by the emitter and drives the cameras. The software also comprises many other modules such as system calibration, extracting light stripes, finding correspondence, reconstruction, display, and so on. The structured light patterns are controlled by the computer.

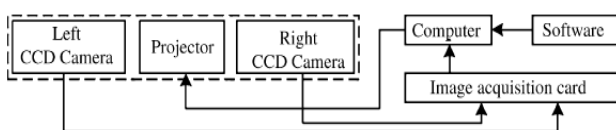


Fig. 1. Structure of measurement system.

3. SYSTEM CALIBRATION

Before the system works, cameras' internal parameters and structure parameters between cameras must be calibrated (Remondino, 2006 and Gruen, 2001). Then, we may begin to measure an object.

For the efficiency of our active photogrammetric system it is important, how accurate the camera geometry is known. Since we used a standard stereo camera setup, the system can be calibrated using a planar test field and a convergent setup. In order to increase accuracy and to ease calibration, we do separate intrinsic calibration of each camera and then do an extrinsic calibration step.

3.1 Intrinsic Calibration

Our test field consists of a wooden plate, on which we fixed a sheet of self-adhesive paper showing a planar object point array, namely a black and white checkerboard pattern. On the pattern there are also four tiny squares with different colours which allow us to determine the orientation of the test field (Figure.2).

In the first step each of the two cameras separately be moved around the planar test field and capture images from different views and distances based on a predefined design for camera settings and all camera stations called photogrammetric network design for camera calibration (Fraser, 1996).



Figure. 2. The planar target for calibration.

The black and white squares on the planar test field are processed and all visible feature points (the corners of black and white squares with the same size) are measured and identified fully automatically by Harris corner detector (Harris, 1998). These measurements are used to compute the bundle solution for the calibration parameters externally using the *Australis* software package from *The Department of Geomatics of The University of Melbourne* based on self-calibration bundle adjustment method. Our cameras are modeled with 10 parameters, namely the focal length c , the principal point offsets x_o and y_o , K_1 , K_2 and K_3 for radial symmetric distortion, P_1 , P_2 for decentering distortion and finally B_1 and B_2 for scale and shear. Accurate space coordinates for the control field points are also obtained.

3.2 Extrinsic Calibration And Essential Matrix Derivation

After determining intrinsic parameters of each camera, they are mounted on a stable aluminum profile with a fixed convergent setup while multi-media video projector has already been fixed between them. In order to determine relative

orientation parameters between two cameras the planar checkerboard is used. Each of the cameras captures an image. All of the corners points on checkerboard that now have an accurate 3D coordinate from the bundle adjustment in previous step are used as 3D control points in order to determine six exterior orientation parameters of each of the two cameras based on collinearity equations.

$$\begin{aligned} x_i - x_o + \Delta x &= \frac{-c[m_{11}(X_o - X_i) + m_{12}(Y_o - Y_i) + m_{13}(Z_o - Z_i)]}{[m_{31}(X_o - X_i) + m_{32}(Y_o - Y_i) + m_{33}(Z_o - Z_i)]} \\ y_i - y_o + \Delta y &= \frac{-c[m_{21}(X_o - X_i) + m_{22}(Y_o - Y_i) + m_{23}(Z_o - Z_i)]}{[m_{31}(X_o - X_i) + m_{32}(Y_o - Y_i) + m_{33}(Z_o - Z_i)]} \end{aligned} \quad (3-1)$$

where x_i and y_i are image coordinates of the i^{th} corner point of the checkerboard. x_o and y_o are coordinates of the principal point offsets and c is calibrated focal length. Δx and Δy are corrections to x_i and y_i respectively to remove all systematic errors that are known from camera calibration. $m_{11}, m_{12}, \dots, m_{33}$, are nine coefficients of the orthogonal transformation between the image plane orientation and object space orientation, and are functions of the rotation angles ω, ϕ , and κ which are unknown. X_o, Y_o, Z_o , are the object space coordinate of the camera position which are unknown. X, Y, Z , are space coordinates of each corner point on the checkerboard that are used as accurate 3D control points that are known from bundle adjustment self calibration in section 3.1.

Since these equations are non-linear they are first linearized by the use of a Taylor's series expansion of the function with respect to each of the unknown elements.

$$\begin{aligned} x_i - x_o + \Delta x + v_{x_i} &= b_{11}d\omega + b_{12}d\phi + b_{13}d\kappa - b_{14}dX_o - b_{15}dY_o - b_{16}dZ_o + F_o \\ y_i - y_o + \Delta y + v_{y_i} &= b_{21}d\omega + b_{22}d\phi + b_{23}d\kappa - b_{24}dX_o - b_{25}dY_o - b_{26}dZ_o + G_o \end{aligned} \quad (3-2)$$

where F_o and G_o are the evaluation of the original functions with estimated values of the unknowns. b_{ij} indicate the partial derivative coefficients of the original equations for the respective unknown. v_x and v_y are residuals to image coordinates from the least squares solution when there are more equations than unknowns.

Let $\vec{o}_1 = (X_o, Y_o, Z_o)_1^T$ and $\vec{o}_2 = (X_o, Y_o, Z_o)_2^T$ be camera positions in checkerboard (or object) coordinate system for left and right cameras, respectively. Then we can define base vector between two cameras \vec{T}_b as

$$\vec{T}_b = \vec{o}_2 - \vec{o}_1 = \begin{pmatrix} b_x & b_y & b_z \end{pmatrix}^T \quad (3-3)$$

The orientation of each camera with respect to the object coordinate system can be obtained as an orthogonal rotation matrix as

$$M_i = \begin{pmatrix} \cos \phi_i \cos \kappa_i & \cos \omega_i \sin \kappa_i + \sin \omega_i \sin \phi_i \cos \kappa_i \\ -\cos \phi_i \sin \kappa_i & \cos \omega_i \cos \kappa_i - \sin \omega_i \sin \phi_i \sin \kappa_i \\ \sin \phi_i & -\sin \omega_i \cos \phi_i \\ & \sin \omega_i \sin \kappa_i - \cos \omega_i \sin \phi_i \cos \kappa_i \\ & \sin \omega_i \cos \kappa_i + \cos \omega_i \sin \phi_i \sin \kappa_i \\ & \cos \omega_i \cos \phi_i \end{pmatrix} \quad (3-4)$$

where $i=1,2$.

Then essential matrix is given by

$$E' = M_1 K_b M_2^T \quad (3.5)$$

where K_b is the base matrix as

$$K_b = \begin{pmatrix} 0 & -b_z & b_y \\ b_z & 0 & -b_x \\ -b_y & b_x & 0 \end{pmatrix} \quad (3.6)$$

3.3 Project E' On To The Essential Space

The following theorem, due to Huang and Faugeras, 1989, captures the algebraic structure of essential matrices in terms of their singular value decomposition.

A nonzero matrix $E \in \mathfrak{R}^{3 \times 3}$ is an essential matrix if and only if E has a singular value decomposition (SVD):

$$E = U \Sigma V^T \quad (3.7)$$

with $\Sigma = \text{diag}\{\sigma, \sigma, 0\}$ for some $\sigma \in \mathfrak{R}_+$ and $U, V \in SO(3)$.

where $SO(3)$ is the space of all special orthogonal matrices in $\mathfrak{R}^{3 \times 3}$ that is usually denoted by

$$SO(3) = \left\{ R \in \mathfrak{R}^{3 \times 3} \mid R^T R = I, \det(R) = +1 \right\}. \quad (3.8)$$

Given a real matrix $F \in \mathfrak{R}^{3 \times 3}$ with

$$SVD F = U \text{diag}\{\lambda_1, \lambda_2, \lambda_3\} V^T \quad (3.9)$$

with $U, V \in SO(3)$, $\lambda_1 \geq \lambda_2 \geq \lambda_3$ then the essential matrix E

that minimizes the error $\|E - F\|_f^2$ is given by

$$E = U \text{diag}\{\sigma, \sigma, 0\} V^T \quad (3.10)$$

with

$$\sigma = (\lambda_1 + \lambda_2) / 2 \quad (3.11)$$

where the subscript f indicates the Frobenius norm of a matrix. This is the square norm of the sum of the squares of all the entries of the matrix (Figure.3).

Base on the above theorem we compute the singular value decomposition of the matrix E' computed in the previous section as

$$SVD E' = U \text{diag}\{\sigma_1, \sigma_2, \sigma_3\} V^T \quad (3.12)$$

In general, since E' may not be an essential matrix, then $\sigma_1 \neq \sigma_2$ and $\sigma_3 \neq 0$.

But its projection onto the normalized essential space is

$$E = U \Sigma V^T \quad (3.13)$$

where

$$\Sigma = \text{diag}\{1,1,0\} \quad (3.14)$$

In order to improve the accuracy of the essential matrix and to remove the effect of any noise during the measurements an optimization step based on the least squares minimization of the following objective function is done

$$\Sigma(x_1^j, x_2^j)^T E x_2^j)^2 \rightarrow \min, \quad (j=1,2,\dots,n) \quad (3.15)$$

where x_1^j and x_2^j are refined image coordinates of n conjugate points in left and right images, respectively.

The essential matrix E contains information about the relative position T and orientation $R \in SO(3)$ between the two cameras as:

$$E = \tilde{R} T \in \mathfrak{R}^{3 \times 3} \quad (3.16)$$

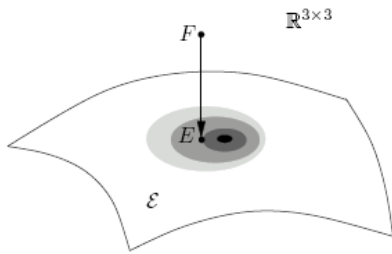


Figure.3. Among all points in the essential space $\varepsilon \subset \mathfrak{R}^{3 \times 3}$, E has the shortest Frobenius distance to F .

4. EXTRACTING LIGHT STRIP

It is important for the system to extract the exact centers of the light stripe because it can affect the precision of 3D measurement. The usual approach detects light stripes by considering the gray values of the image. For example, the point with the highest brightness is considered as the center point of light stripe. Furthermore, the stripe's centroids are often used as the center point. None of these methods can extract light stripe in sub-pixel. In this paper, a method of extracting light stripe in sub-pixel is given.

The method to extract light stripe in sub-pixel is to regard image pixel gray value z as the function about image pixel coordinate (x, y) , namely $z(x, y)$, and extract light stripes from it by using differential geometric properties. The basic idea behind these algorithms is to locate the positions of ridges and ravines in the image function. Based on this idea (Steger, 1998) brings forward a method extracting light stripe in sub-pixel. Let $s(t)$ be the light stripe, $s'(t)$ be the first derivative, namely the tangent direction, and $n(t) = (n_x, n_y)^T$ be the norm direction. Along $n(t)$, those points whose first derivatives are zero and second derivatives' absolute value are the maximum are considered as the centers of the light stripe. Let r be the locally estimated value of $z(x_0, y_0)$, and $r_x, r_y, r_{xx}, r_{xy}, r_{yy}$ be the locally estimated derivatives at

point (x_0, y_0) that are obtained by convolving the image with Gaussian convolution masks. Then, the Taylor polynomial of the image function $z(x, y)$ at point (x_0, y_0) is given by

$$f(tn_x + x_0, tn_y + y_0) = r + tn_x r_x + tn_y r_y + \frac{1}{2} t^2 n_x^2 r_{xx} + t^2 n_x n_y r_{xy} + \frac{1}{2} t^2 n_y^2 r_{yy} \quad (4.1)$$

The norm direction $n(t)$ is calculated through a so-called Hessian matrix defined as

$$H(x, y) = \begin{pmatrix} r_{xx} & r_{xy} \\ r_{xy} & r_{yy} \end{pmatrix} \quad (4.2)$$

Its eigenvector corresponding to the maximum eigenvalue is equal to the $n(t)$. Let $(\partial f / \partial t)(tn_x + x_0, tn_y + y_0) = 0$, we can obtain

$$t = -\frac{n_x r_x + n_y r_y}{n_x^2 r_{xx} + 2n_x n_y r_{xy} + n_y^2 r_{yy}} \quad (4.3)$$

The center points of light stripes are

$$(p_x, p_y) = (tn_x + x_0, tn_y + y_0) \quad (4.4)$$

where $-1/2 \leq m_x \leq 1/2, -1/2 \leq m_y \leq 1/2$ are required.

Figure 4 shows the image of a measured object when multi-line structured light is projected on it (left) and the extracted centers of light stripes by this approach.

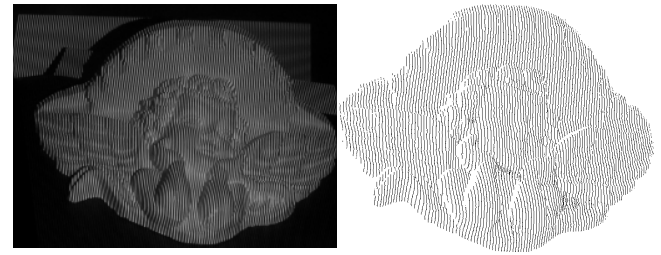


Figure 4: Multi-line light stripes image projected on the statue (left) and the extracted centers of stripes (right).

5. FINDING CORRESPONDENCE

In order to simplify stereo match, the technology of line shift processing which first proposed by Guhring in 2001, is applied to stereo vision system to increase feature information on the measured surface. Since a multi-stripe pattern is a periodic pattern (of discrete nature), the projection of coding patterns are also required in order to solve the ambiguities that arise. Then, given a light stripe point with certain code on left image, we search the correspondent point along the light stripe with the same code on right image. The searching process is stopped when the point meets epipolar constraint. Thus, the correspondences are found. We will introduce our coding strategy and the matching method, respectively, as follows.

5.1 Coding Strategy

For structured light analysis, projecting a Gray code is superior to a binary code projection. On the one hand, successive numbers of the Gray code vary exactly in one bit. Thus, wrong decoding which is most likely to occur at locations where one bit switches, introduces only a misplacement of at most one resolution unit. On the other hand, the width of bright and dark lines in the pattern with finest resolution is twice as wide compared to the binary code. This facilitates analysis especially at steep object surfaces where the code appears to be

compressed. Since we make use of a per pixel varying threshold, the Gray code solution is very robust.

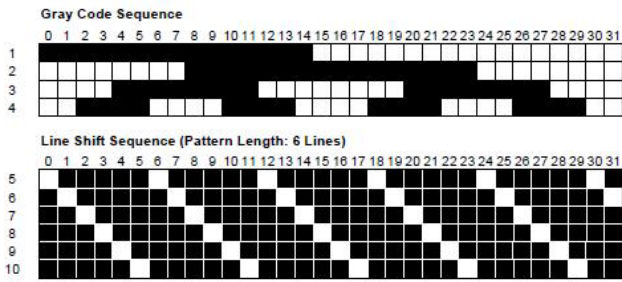


Figure 5: Line shifting technique: Gray code and line shifting patterns for 32-pixel-wide patterns

With regard to the Gray coded patterns, a total number of n regions should be labeled, being n the number of lines projected in every line shifting pattern. Therefore, every pattern area where a line is shifted has its own label or code (Figure. 5).

In our experiment with regard to the projector's resolution (1024×728), we chose $n=128$. Therefore, 128 bands of eight pixels width should be labeled by seven Gray code patterns. In this case the distance between consecutive lines in one image is two times the resolution of the Gray code. We decided to introduce an oversampling technique consisting of projecting an additional Gray coded pattern (8th Gray coded pattern) to establish support regions during the labeling process, yielding a more robust solution to codification the regions.

Totally 18 patterns are projected onto the measuring surface: eight vertical Gray codes; eight vertical multi-stripe patterns, each one shifted a column towards the right; two additional patterns for grey level normalisation (one fully illuminated and the other with the lamp switched off).

5.2 Matching

Figure 6 shows the method of finding correspondences based on coded structured light. Having being encoded, every light stripe in left and right image has a unique codeword. The light stripes with the same codeword in two images are spatially located at the same position. Let L_i and R_i be the point set with the codeword i ($i = 1, 2, \dots, N$, N is the number of stripes) in left and right images, respectively. Select any point $p_l \in L_i$, and the correspond point p_r in right image meets $p_r \in R_i$. According to epipolar constraint [23], we have

$$\tilde{p}_l \cdot \mathbf{E} \cdot \tilde{p}_r = 0 \quad (5.1)$$

where \tilde{p}_l and \tilde{p}_r are normalized coordinates of the points on images, and \mathbf{E} is the essential matrix. In term of above two constraints, we can uniquely ascertain the correspondent point p_r in right image of point p_l in left image.

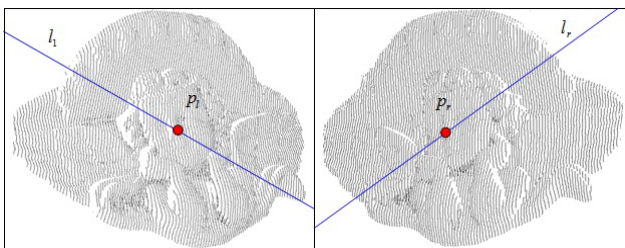


Figure 6: Coded structured light matching method



Figure 7: The designed vision sensor



Figure 8: The Images of an Angel statue captured by left and right cameras.



Figure 9: Images of the 5th Gray code pattern captured by left and right cameras.

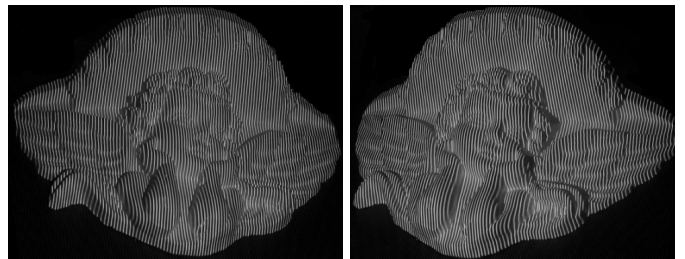


Figure 10: Images of the first multi-line scanning pattern captured by left and right cameras.

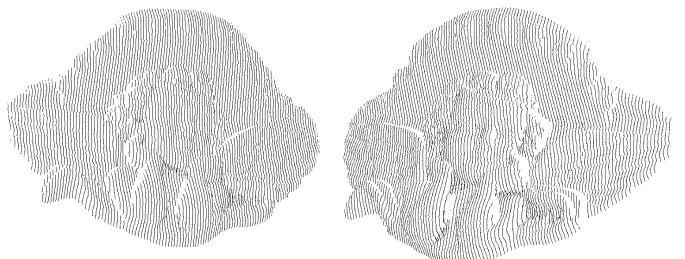


Figure 11: Light stripe centers extracted from the first left and right multi-line scanning images.



Figure12 : 3D reconstruction result using 1024 light stripes.

6. EXPERIMENTAL RESULTS

6.1 Measuring an Angel statue

This section reports some tests to assess the performance of the measurement system. Figure 7 shows the factual vision sensor. Two common digital cameras (Canon Power shot G3) constitute a stereo vision sensor. A DLP multimedia projector (Infocus X2) is used to project structured light patterns.

The measured object is an Angel statue, which is about 500mm tall and 700mm wide (Figure. 8). The projector projects eight scanning patterns based on multi-line shift processing. Each scanning pattern contains 128 light stripes. Then, each light strip in the multi-line scanning patterns is encoded by the Gray code method. Figure. 9 shows the images of the 5th Gray code pattern projected on the Angel statue and captured by left and right cameras. The first scanning multi-line shift pattern projected on the statue captured by left and right cameras are shown in Figure. 10.

The light stripe centers of the first multi-line scanning pattern are extracted as shown in Figure 11. According to the eight coding patterns, they are encoded as 11111111, 11111110, 11111101, . . . , and 00000000 from left to right. Likewise, the light stripe centers of the seven other multi-line scanning patterns are also encoded as the same results. There are 527012 light stripe centers having been encoded in our experiment, and the number of error codewords is approximately 500, so the error codeword ratio is only about 0.1%.

The Angel statue is then triangulated after matching. The 3D data is shown in Figure 12, which shows the reconstruction result using 1024 light stripes.

6.2 Testing Performances

To test the system performance, we conducted an experiment by measuring the planar target. The images captured by left and right cameras are used for 3D reconstruction of feature points of the planar target. The differences between calculated 3D coordinates of the feature points with ones from the test field calibration are used for evaluating the performance of the stereo vision sensor. 3D data of the feature points obtained in two ways should be theoretically equal. According to this, we evaluate the sensor performance. The RMS errors of X, Y, Z coordinates are 0.035 mm, 0.024 mm, 0.120 mm respectively.

7. CONCLUSION

We have developed a low cost 3D scanner based on integration of close range photogrammetry and Gray coded structured light together with multi-line shift processing principle. The scanner has been implemented and tested on a real, complex artwork and produced good results. This low cost scanner is capable to generate dense and high accurate point cloud from complex object surfaces. The experimental results have indicated that the ratio of error codeword and consequently error matching is only 0.1%.

The comparison of the 3D feature point coordinates of the test field, reconstructed based on this stereo vision system and ones from test field calibration verifies the accuracy of the essential matrix derivation method. Based on this accurate essential matrix, given a light stripe point on left image, the correspondent point on right image is the intersections of coded light stripes with same code and corresponding epipolar line.

Calibration of the intrinsic and extrinsic parameters of the cameras is achieved using well-known photogrammetric techniques.

The advantages of this system lie in its design simplicity, low cost and the potential for fast and robust implementation.

References

- Fraser, C.S. 1996. Network Design. In K.B. Atkinson, editor, *Close Range Photogrammetry and Machine Vision*, chapter 9, pages 256-281. Whittles Publishing, Roseleigh House, Latheronwheel, Caithness, KW5 6DW, Scotland, UK.
- Fusiello, A, Roberto. V and Trucco, E, 1997. Efficient Stereo with Multiple Windowing, in *IEEE Int'l Conference on Computer Vision and Pattern Recognition*, pp. 858-863.
- Gruen A. and Beyer, H.A., 2001. System calibration through self-calibration. In 'Calibration and Orientation of Cameras in Computer Vision' Gruen and Huang (Eds.), Springer Series in Information Sciences 34, 163-194
- Guhring, J, 2001. Dense 3-d surface acquisition by structured light using of-the-shelf components, *Videometrics Opt. Meth. 3D Shape Meas.* 4309, 220-231.
- Harris, C, Stephens. M. 1988. A combined corner and edge detector, in: *Proceedings of 4th Alvey Vision Conference*, Manchester, UK, 147-151.
- Huang. T.S, Faugeras. O.D, 1989. Some properties of the E matrix in two-view motion estimation. *IEEE Transactions on Pattern Analysis and Machine Intelligence*, December 11(12):1310-1312.
- Remondino, F., Fraser, C.S., 2006. Digital camera calibration methods: considerations and comparisons. *IAPRS volume XXXVI*, (September 2006) part 5, Dresden, 25-27.
- Salvi, J, Pag`es. J and Batlle, J, 2004. Pattern codification strategies in structured light systems. *Pattern Recognition*, 37(4) 827-849.
- Sun. C, 1997. A Fast Stereo Matching Method, in *Digital Image Computing: Techniques and Applications*, pp. 137-148.